JOURNAL OF GEOPHYSICAL RESEARCH, VOL. 112, A12308, doi:10.1029/2007JA012592, 2007

Polarization measurements of Saturn Electrostatic Discharges with Cassini/RPWS below a frequency of 2 MHz

G. Fischer,[1] D. A. Gurnett,[1] A. Lecacheux,[2] W. Macher,[3] and W. S. Kurth[1]

Received 13 June 2007; revised 28 August 2007; accepted 5 October 2007; published 29 December 2007.

[1] Early in 2006 the RPWS (Radio and Plasma Wave Science) instrument and the ISS (Imaging Science Subsystem) onboard the Cassini spacecraft detected a lightning storm on Saturn that lasted for about one month. The RPWS measured the so-called SEDs (Saturn Electrostatic Discharges), which are high frequency radio signals produced by lightning discharges. The ISS imaged a remarkable cloud system associated with these SEDs at a latitude of 35° South. Below the frequency of 1825 kHz the RPWS was in a mode capable of measuring the polarization of the SEDs. A surprising result was gained; SEDs appeared to be highly polarized (80%) and were exclusively right-handed polarized with a high degree of circular polarization. We will present an explanation for this diagnosis involving magneto-ionic modes and their differential absorption in the magnetoplasma of Saturn's ionosphere.

Citation: Fischer, G., D. A. Gurnett, A. Lecacheux, W. Macher, and W. S. Kurth (2007), Polarization measurements of Saturn Electrostatic Discharges with Cassini/RPWS below a frequency of 2 MHz, *J. Geophys. Res.*, *112*, A12308, doi:10.1029/2007JA012592.

1. Introduction

[2] In this paper we present the results and a consistent interpretation of the first polarization measurements of Saturn Electrostatic Discharges (SEDs) performed by Cassini/RPWS. The polarization of SEDs was a controversial issue in the years following the two Voyager encounters with Saturn. In the very first SED paper *Warwick et al.* [1981] conclude that SEDs might be unpolarized since the signals in the two channels of the Voyager PRA (Planetary Radio Astronomy) instrument look virtually identical, and the two channels measure opposite senses of circular polarization. However, they also note that some SEDs occurring in episodes after Voyager 1 closest approach do show polarization. *Evans et al.* [1981, Figure 5] plot an index of polarization for the SEDs of the Voyager 1 first post-encounter episode as a function of frequency showing that the SEDs are strongly left-circularly polarized above ~15 MHz. Below this frequency, the degree of circular polarization is much less, and the sense looks frequency-dependent. On the other hand, *Zarka and Pedersen* [1983] contend that the polarization determination by *Evans et al.* [1981] takes into account neither the geometrical orientation of the Voyager PRA antennas with respect to the source, nor the distortion of antenna lobes at higher frequencies. A theoretical antenna response model of the Voyager antennas by *Ortega-Molina and Daigne* [1984] shows that there should be a polarization reversal around 15 MHz due to multibeamed antenna patterns at these high frequencies, so the apparent polarization determined by *Evans et al.* [1981] for the high frequencies should be just due to an instrumental effect. *Zarka and Pedersen* [1983] note that the SED emission might be unpolarized, and that any attempt to characterize the polarization of SEDs must take into account all instrumental problems.

[3] In section 2 of this paper we will describe the RPWS antenna system and data analysis, and we will quickly review the characterization of the polarization state of a radio wave by means of the Stokes parameters in section 3 and in the appendix. In the polarization analysis of Cassini/RPWS data in section 4 we will take into account all instrumental parameters as well as the exact antenna-source geometry. In section 5 we will try to give a theoretical explanation for the surprising result of the RPWS SED polarization measurements. In the final discussion we will also compare our result to polarization measurements of radio emissions from terrestrial lightning.

2. RPWS Antenna System and Data Analysis With Respect to Polarization Measurements

[4] The RPWS has three monopole antennas E_u, E_v, E_w of 10 m in length for electric field measurements and receivers for various frequency ranges [*Gurnett et al.*, 2004]. The RPWS antenna system has been calibrated by three different methods, an experimental method called rheometry with a Cassini scale model [*Rucker et al.*, 1996], a numerical computer simulation called wire-grid modeling [*Fischer et*

[1]Department of Physics and Astronomy, University of Iowa, Iowa City, Iowa, USA.
[2]Observatoire de Paris–Meudon, Meudon Cedex, France.
[3]Space Research Institute, Austrian Academy of Sciences, Graz, Austria.

0148-0227/07/2007JA012592$09.00

al., 2001], and finally in-flight calibration with Jovian radio sources [*Vogl et al.*, 2004; *Cecconi and Zarka*, 2005]. In these calibrations the so-called effective length vector of each antenna was determined, a knowledge that is essential for direction finding and polarization measurements of incoming radio waves. However, this calibration can only be used in the so-called "quasistatic" frequency range, where the short dipole approximation is valid and the wavelength is significantly longer than the dimensions of the spacecraft. At quasistatic frequencies the antenna pattern of the RPWS monopoles (the spacecraft forms the "ground" or the second dipole arm) is the typical doughnut shaped torus, where the effective length vector points in the direction of minimum antenna gain [*Fischer et al.*, 2003]. At higher frequencies this torus is distorted resulting in a complex effective length vector that depends on frequency as well as the direction of the incoming wave. This behavior can be fairly described by the numerical method of wire-grid modeling and the transition from the quasistatic frequency regime to the higher frequencies is a gradual one. It was found by wire-grid modeling that the results of the RPWS antenna calibration for the quasistatic frequency range can be used up to a frequency of about 2 MHz.

[5] Early 2006 the RPWS instrument recorded the SEDs of a giant lightning storm, which was named storm E by *Fischer et al.* [2007]. The HFR (High Frequency Receiver) of the RPWS instrument measured the SED signals in its HF1 and HF2 bands. In both bands the receiver sweeps from low to high frequencies with an instantaneous bandwidth of 25 kHz, and it can be programmed to use different frequency step sizes and integration times. During the SED storm E HF1 swept from 325 to 1800 kHz with 60 frequency steps of a step size of 25 kHz. The 25 kHz passband was digitally filtered to provide two linear channels with a frequency resolution of 12.5 kHz. HF2 swept from 1825 to 16025 kHz in 143 frequency steps of a size of 100 kHz. In HF2 the measurement was performed only by the dipole E_x, which can be formed by the two monopole antennas E_u and E_v, hence it is not possible to determine the polarization. However, in the HF1 band RPWS used two antennas, the dipole E_x as well as the monopole E_w, and an integration time of 80 ms was used. In HF1 the instrument was in the so-called polarimeter mode measuring the auto-correlations of the dipole $\langle V_x V_x^* \rangle$ and the monopole $\langle V_w V_w^* \rangle$ as well as the real and imaginary part of the cross-correlation ($Re\langle V_x V_w^* \rangle$ and $Im\langle V_x V_w^* \rangle$). This is sufficient to unambiguously determine the polarization in case the direction of the source and the orientation of the antennas with respect to the source are known.

[6] Several convincing arguments that SEDs are the radio signatures of lightning storms in Saturn's atmosphere were recently given by *Fischer et al.* [2007], so we can simply assume that Saturn is the source of the SEDs. More precisely, *Dyudina et al.* [2007] show images of a prominent cloud feature at a planetocentric latitude of 35° South whose occurrence and rotation rate is consistent with the SEDs from storm E early 2006. As Cassini was relatively distant during this SED storm it is enough to take the center of Saturn as seen from Cassini as the source direction. The closest distance of Cassini during which SEDs were recorded in HF1 was about 27 R_S (Saturn radii) from the center of Saturn, resulting in a maximum error of $\arctan(1/27) \approx 2.1°$ in case the storm system is located at the planet's limb. For more than 80% of all SEDs recorded in HF1 the distance of Cassini was more than 44 R_S corresponding to a maximum error for the source direction of only 1.3°. This error is of the order of the antenna calibration error, which is around 2° [*Cecconi and Zarka*, 2005]. The error of the direction of the assumed source is even less for many HF1 recorded SEDs, as most of them were recorded when the storm system was close to the central meridian on the nightside of the planet. As the ionospheric cutoff frequency on the dayside of Saturn is around 5 MHz [*Kaiser et al.*, 1984] the SEDs were only detected in HF1 (below ~2 MHz) when the storm was on the nightside. In the course of the SED polarimeter measurements the Cassini spacecraft was located from 3.1 to 7.6 LT (local time), i.e., on the early morning side of the planet.

[7] The extraction of SEDs from RPWS data has been already described in detail by *Fischer et al.* [2006]. For the dipole measurement (E_x) in the HF1 band an intensity threshold of 1.6 dB (corresponding to 4 standard deviations of the background fluctuation) was used to extract about 1600 SEDs for the SED storm E [*Fischer et al.*, 2007]. These SEDs consist of about 2800 SED "pixels" (one flux measurement at a certain frequency channel and time), as some of them extend over several frequency channels within their duration. We reduced this data set first to about one quarter (slightly more than 400 SEDs consisting of more than 700 SED pixels) by the additional requirement that the intensity of the monopole (E_w) measurement should be as well greater than 1.6 dB above the galactic background. We note that several frequency channels in HF1 have an increased noise level and could not be used for SED polarization measurements. These were mainly the two channels adjacent to all 100 kHz harmonics as well as the channels of 1343.75 and 1356.25 kHz.

[8] The lowest SED frequency in the reduced data set is 918.25 kHz and the highest is in the channel centered at 1781.25 kHz. This is adequately within the quasistatic frequency range. For the directions of the effective antenna length vectors we used the calibrated values in Table 5 of *Vogl et al.* [2004] with the effective antenna lengths given by *Zarka et al.* [2004], which are $h_x = 3.06$ m for the dipole E_x and $h_w = 1.68$ m for the monopole E_w, respectively. We assume the center of Saturn to be the source, and we do know the geometry of the antenna system with regard to the source as given by Cassini attitude data. Hence we will determine the real polarization of the SEDs (not just the apparent one) as our analysis includes all instrumental parameters and does take into account the antenna-source geometry.

[9] One factor to be mentioned which is limiting the accuracy of polarization measurements is the angle β of the source to the antenna plane, which should not be too small. The antenna plane for our measurements is defined by the effective axes of the E_x dipole and the E_w monopole. The former is nearly identical to the x axis of the standard Cassini coordinate system (see Figure 1), whereas the latter is given by the azimuth $\phi_w = 90.3°$ and the colatitude $\theta_w = 29.4°$ [*Vogl et al.*, 2004]. About half of the SEDs in our data set were obtained when the source (Saturn) was positioned in the negative y-direction, as the non-rotatable ISS cameras are pointed in that way. For this position the angle β is

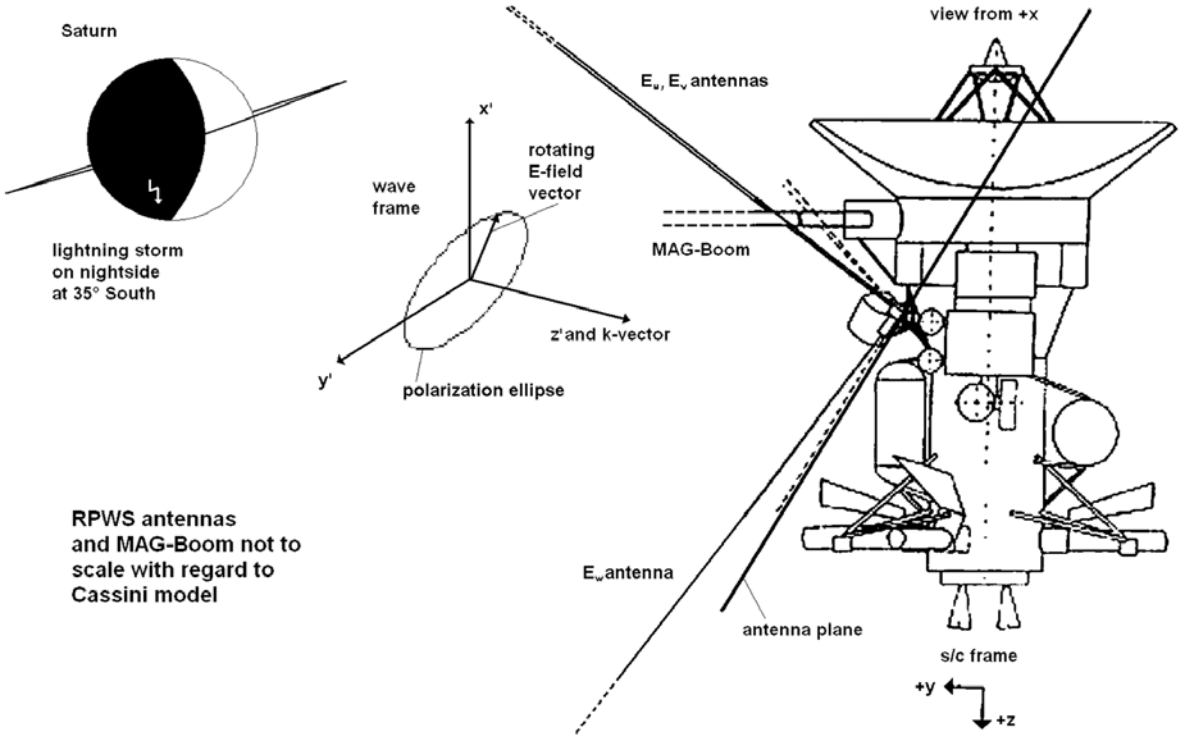

Figure 1. Sketch showing the SED polarization measurement situation: A radio wave originating from a lightning flash from Saturn's nightside has a polarization ellipse shown in the wave frame (x′, y′, z′). It arrives at Cassini where the antenna plane formed by the effective axes of E_x dipole and E_w monopole is indicated. Sketch of Cassini spacecraft was adapted from *Rucker et al.* [1996]. It is a view along the *x* axis of the s/c frame (identical with effective axis of E_x dipole).

around 60°, which is not bad with regard to polarization measurements. Similarly, for about 30% of SEDs Saturn was located at the other side of the antenna plane at angles $\beta > 60°$. The latter situation is approximately sketched in Figure 1. Finally, we applied a more stringent criterion than *Cecconi et al.* [2006] for polarization measurements and excluded all SED measurements with $\beta < 40°$. This final step reduced our data set to 665 SED pixels, whose polarization characteristics will be presented in section 4.

3. Short Description of the Polarization of Electromagnetic Waves and Stokes Parameters

[10] Before presenting the main results of the RPWS SED polarization measurements we will shortly describe some basics of wave polarization. For the description of the polarization state of a wave it is convenient to introduce a special orthogonal coordinate system called the wave frame. It is displayed in Figure 1 showing a sketch of the measurement situation. Without loss of generality one can introduce the z'-axis of this system parallel to the wave vector $\vec{k}$, and the x' and y'-axis lie in a plane normal to $\vec{k}$. There is one degree of freedom, because one can choose any direction in this plane for the x'-axis or y'-axis. However, once it is chosen, the third axis is automatically fixed due to the required orthogonality and right-handedness. The polarization state of the general case of an elliptically polarized wave is often described as a superposition of two linearly polarized waves, one polarized in the x′-direction ($E_{x'}$) and the other in the y′-direction ($E_{y'}$) [*Kraus*, 1986]:

$$E_{x'} = E_1 \sin(\omega t) \text{ and } E_{y'} = E_2 \sin(wt + \delta), \tag{1}$$

with E_1 and E_2 as wave amplitudes. The angular wave frequency is denoted by ω, t is the time, and δ the phase difference. The polarization ellipse can also be described by two angles ε and τ, where ε describes the amplitude ratio and τ the tilt angle of the polarization ellipse, respectively. The two angles 2ε and 2τ also represent the latitude and longitude on the Poincaré sphere, which is a convenient way to describe a particular polarization state of an electromagnetic wave. The cartesian coordinates of this polarization state (measured from the central point of the Poincaré sphere) are the well-known Stokes parameters (Q, U, V), and the intensity I is its radius. The Stokes parameters can be expressed by the following equations [*Kraus*, 1986]:

$$\begin{aligned} I &= \langle E_1^2 \rangle + \langle E_2^2 \rangle = S \\ Q &= \langle E_1^2 \rangle - \langle E_2^2 \rangle = S\langle \cos(2\epsilon)\cos(2\tau) \rangle \\ U &= \langle 2E_1E_2\cos(\delta) \rangle = S\langle \cos(2\epsilon)\sin(2\tau) \rangle \\ V &= \langle 2E_1E_2\sin(\delta) \rangle = S\langle \sin(2\epsilon) \rangle \end{aligned} \tag{2}$$

with $\langle \ldots \rangle$ as a time averaging operation and S or I as the total flux density. The latter is measured in units of $V^2/(m^2\ Hz)$ or can be transformed to $W/(m^2\ Hz)$ by a division by the impedance of free space $Z = 120\pi$ ohms. The equation $I^2 =$

$Q^2 + U^2 + V^2$ represents the condition for a completely polarized wave. However, in reality waves are often only partially polarized. In this case we have $I^2 > Q^2 + U^2 + V^2$, and it is convenient to define the degree of polarization d:

$$d = \frac{\sqrt{Q^2 + U^2 + V^2}}{I} \tag{3}$$

[11] The polarized part of the wave can be decomposed into a degree of linear polarization d_l and a degree of circular polarization d_c:

$$d_l = \frac{\sqrt{Q^2 + U^2}}{I} \quad \text{and} \quad d_c = \frac{V}{I}, \tag{4}$$

and we have $d^2 = d_l^2 + d_c^2$. We note that the Stokes parameters Q and U depend on the choice of the coordinate axes x′ and y′, because different axes will result in different polarization ellipse tilt angles τ (the degree of freedom we mentioned at the beginning of this section). On the other hand, the degree of linear as well as the degree of circular polarization (d_l and d_c) do not depend on the choice of x′ and y′ axes of the wave frame. In this paper we use the radioastronomical and IRE (Institute of Radio Engineers) definition of the polarization sense [*Kraus*, 1986], i.e., a LH (left-handed) wave rotates clockwise for an observer to whom the wave is approaching, or a LH wave is radiated from a LH helical antenna and rotates counterclockwise when receding.

[12] In magneto-ionic theory the polarization of the magneto-ionic mode waves is often described by one complex number p, which is further elaborated in the appendix of this paper.

4. RPWS Measurements of SED Polarization Measurements

[13] The calculation of the normalized Stokes parameters q, u, v, and the flux S can be done with the following linear system of equations:

$$\begin{pmatrix} \langle V_w V_w^* \rangle \\ (h_w/h_x)^2 \langle V_x V_x^* \rangle \\ (h_w/h_x) Re\langle V_x V_w^* \rangle \\ (h_w/h_x) Im\langle V_x V_w^* \rangle \end{pmatrix} = \mathbf{M} \frac{S h_w^2}{2} \begin{pmatrix} 1 \\ q \\ u \\ v \end{pmatrix}, \tag{5}$$

with $\mathbf{M}$ being a 4×4 matrix representing the antenna-source geometry, and h_x and h_w as the effective length of dipole and monopole, respectively, as given in section 2. This equation resembles equation (20) of *Cecconi and Zarka* [2005], and we have only used different symbols for the effective lengths as well as the four measured values $\langle V_x V_x^* \rangle$, $\langle V_w V_w^* \rangle$, $Re\langle V_x V_w^* \rangle$, and $Im\langle V_x V_w^* \rangle$. It is convenient to normalize the Stokes parameters by dividing them by the intensity S, and we use small letters to denote the normalized Stokes parameters, i.e., $q = Q/S$, $u = U/S$, and $v = V/S$. The matrix $\mathbf{M}$ basically consists of the coordinates of each effective antenna unit vector projected onto the wave plane, and the exact equations are discussed by *Cecconi and Zarka* [2005]. Their equation (21) together with their equations (8) and (9) allow the full calculation of $\mathbf{M}$ as antenna and source directions are known in a spacecraft fixed coordinate system. In case the matrix $\mathbf{M}$ is not singular it can be inverted and the four unknown parameters S, q, u, and v can be calculated. We note that for the measured autocorrelation values $\langle V_x V_x^* \rangle$ and $\langle V_w V_w^* \rangle$ a background subtraction has to be applied before the insertion into the equation system above. The background was calculated for each frequency channel and each hour as the mean intensity after elimination of strong signals exceeding four standard deviations.

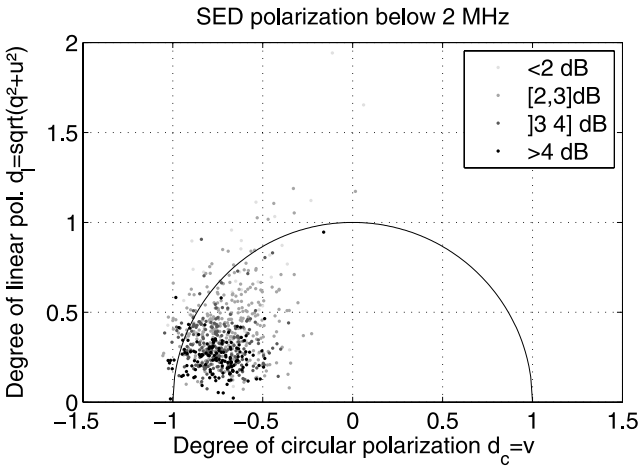

Figure 2. Degree of linear polarization $d_l = \sqrt{q^2 + u^2}$ versus degree of circular polarization $d_c = v$ for SEDs recorded in the HF1 band early 2006. Different intensities of the SEDs (averaged intensity measured by dipole and monopole) are plotted in four different gray scales.

[14] Figure 2 displays the degree of linear polarization $d_l = \sqrt{q^2 + u^2}$ versus the degree of circular polarization $d_c = v$ for our SED data set (each SED pixel is represented by one dot), and it shows a very surprising result. The polarization sense is given by the sign of v and a right-handed (RH) polarized wave has $v < 0$, whereas a left-handed (LH) one has $v > 0$. A right-handed completely circularly polarized wave is given by $d_c = -1$ and $d_l = 0$ [*Kraus*, 1986]. Hence SEDs appear to be highly circularly polarized, and the polarization sense is almost exclusively right-handed! Different SED intensities are displayed in various gray scales and the most intense SEDs (black dots) are clustering around $d_c = -0.75$ and $d_l = 0.25$. The half circle at $q^2 + u^2 + v^2 = 1$ shows the theoretical maximum of the degree of polarization, and only a few SEDs lie outside of this circle. This is due to measurement errors and the main error in the polarization determination comes from the error of the measured intensity values. The absolute error of each autocorrelation measurement adds up to about 0.6 dB (relative to the galactic background), consisting of the fluctuation of the background of 0.4 dB (one standard deviation) and the digitation error of the 8-bit HFR analog to digital converter of about 0.2 dB [*Gurnett et al.*, 2004]. Consequently, low intensity bursts show very high relative errors. Taking only the theoretically allowed bursts with $q^2 + u^2 + v^2 \leq 1$ we arrive at a mean circular polarization degree of $\overline{v} = \overline{d_c} = -0.70$, a mean linear polarization degree of $\overline{d_l} = 0.34$, and a mean polarization degree of $\overline{d} = 0.79$ (or nearly 80%).

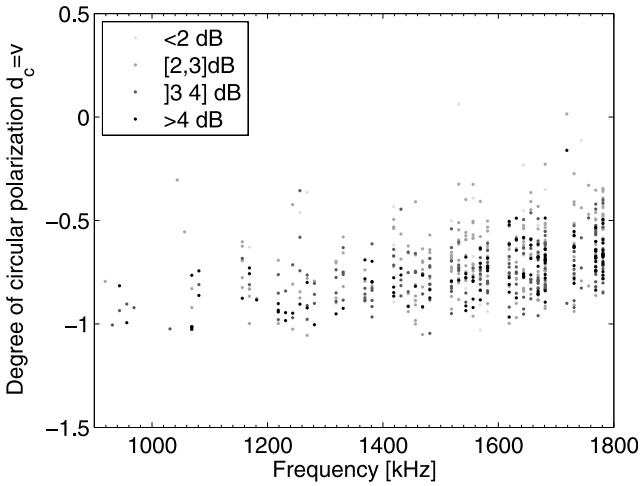

Figure 3. Degree of circular polarization $d_c = v$ as a function of frequency in HF1 for SEDs from early 2006. Different SED burst intensities have different gray scales like in Figure 2.

[15] It is interesting to see if the various degrees of polarization do depend on frequency. Therefore we have plotted the degree of circular polarization d_c versus the SED frequency in Figure 3. Indeed, there seems to be a decrease in the magnitude of circular polarization with $v \approx -0.9$ (nearly a fully circularly RH polarized wave) around 900 kHz to $v \approx -0.6$ around 1800 kHz (with a certain scatter). We also show a similar plot for the degree of linear polarization in Figure 4 showing that the linear polarization degree seems to be approximately constant at its mean value of $\overline{d_l} = 0.34$ throughout the same frequency range. Consequently, the total degree of polarization (not plotted here) is also reduced from about fully polarized ($d = 1$) at 900 kHz to about $d \approx \sqrt{0.6^2 + 0.34^2} \approx 0.7$ at 1800 kHz. This reduction is primarily at the expense of the degree of circular polarization.

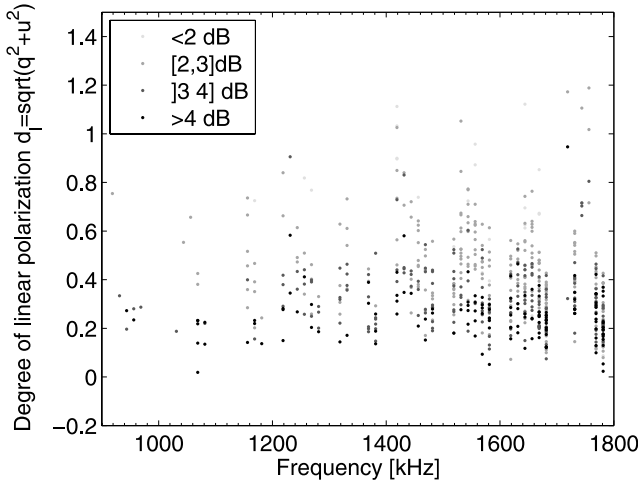

Figure 4. Degree of linear polarization $d_l = \sqrt{q^2 + u^2}$ as a function of frequency in HF1 for SEDs from early 2006. Different SED burst intensities have different gray scales like in Figure 2.

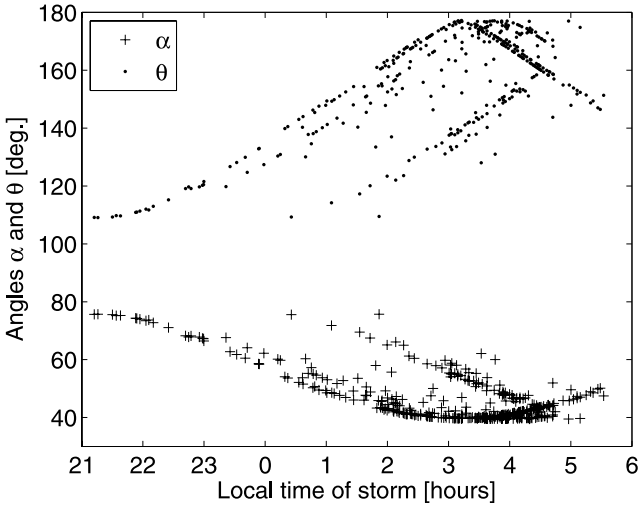

Figure 5. Angle of incidence α between the ionospheric normal and the radio wave and angle θ between the magnetic field and the radio wave direction from the SED source to Cassini are plotted versus the local time of the storm system. Angles α and θ are calculated at an ionospheric altitude of 2000 km and are plotted for each SED in our data set as one cross and as one dot, respectively.

5. An Explanation for the Polarization of SEDs Below 2 MHz

5.1. Geometry of the Problem

[16] Before proceeding to a possible explanation it is helpful to examine the geometry of spacecraft with respect to the SED source. The SEDs in our data set were recorded from DOY 23 to DOY 53, 2006, when Cassini was orbiting Saturn close to its equatorial plane (latitude changed only from 0.14° to −0.29°) at local times (LT) from 3.1 to 7.6 h. We suppose that the SED source is located at a planetocentric latitude of 35° South, where the cameras of Cassini imaged a clearly SED associated cloud feature [*Dyudina et al.*, 2007; *Fischer et al.*, 2007]. This cloud system was located at a Western longitude around 170° on DOY 25 and it drifted westward with a rate around 0.6° per day. Hence the Western longitude $\lambda_{storm}(t)$ (in degrees) of the storm as a function of time can be described by the equation $\lambda_{storm}(t) = 0.6\,t + 155$ with t as the time given in days of year 2006 or fractions thereof. We can easily calculate the local time of the storm $LT_{storm}(t)$ as a function of time with the equation $LT_{storm}(t) = LT_{Cas}(t) + [\lambda_{Cas}(t) - \lambda_{storm}(t)]/15$ as we do know the local time of Cassini $LT_{Cas}(t)$ and its sub-spacecraft Western longitude $\lambda_{Cas}(t)$ as a function of time from Cassini ephemeris data. One can see from Figure 5 that SEDs were only recorded in the HF1 band when the storm was located on the nightside of Saturn from 21 to 6 LT. (In Figure 5 we have plotted only our reduced SED data set, but the previous statement is true for all SEDs recorded below 2 MHz.) For each SED in our data set we have plotted the angles α and θ (as crosses and dots, respectively) versus LT_{storm} in Figure 5. The angle α is the angle of incidence,

which is the angle between the normal of a horizontally stratified ionosphere at an altitude of 2000 km and the radio wave going from the SED source to Cassini, which we assume to propagate in a straight line. This angle was exactly calculated taking into account the oblateness of Saturn. The (average) planetocentric latitude of the point where the radio wave intersects the ionosphere is about 33.5° South corresponding to a planetodetic latitude around 39°. The latter value is close to the minimum of the angle of incidence α, which is reached when the lightning storm is at the central meridian as seen from Cassini. The angle θ indicated as one dot for each SED in Figure 5 is the angle between the magnetic field (also at an altitude of 2000 km exactly where the radio wave from the storm intersects the ionosphere) and the direction of propagation of the radio wave to Cassini.

5.2. SED Radio Waves in the Magnetoplasma of Saturn's Ionosphere

[17] The propagation of a radio wave through a magnetoplasma can be fully described by Appleton's equation (see for example the books by *Ratcliffe* [1959], *Kelso* [1964], or *Budden* [1985]). Its output is the real and imaginary part of the refractive index n as a function of basically five variables, which are the electron plasma frequency f_p (or the electron density N), the wave frequency f, the electron cyclotron frequency f_c, the collision frequency ν, and the angle θ between the direction of propagation and the external magnetic field. Introducing the new variables $X = f_p^2/f^2$, $Y = f_c/f$, $Y_L = -Y\cos(\theta)$, $Y_T = -Y\sin(\theta)$, and $Z = \nu/(2\pi f)$ Appleton's equation can be written as

$$n^2 = 1 - \frac{X}{(1 - jZ) - \frac{Y_T^2}{2(1-X-jZ)} \pm \sqrt{\frac{Y_T^4}{4(1-X-jZ)^2} + Y_L^2}}. \quad (6)$$

[18] In this equation $j = \sqrt{-1}$ represents the imaginary unit, and the electron plasma frequency f_p is linked to the electron density N by the identity $f_p^2 = Ne^2/(4\pi^2 m_e \varepsilon_0)$ with e as the elementary charge, m_e as the mass of an electron, and ε_0 as the permittivity of free space. The electron cyclotron frequency f_c is linked to the magnetic field strength B by the equation $f_c = |e|B/(2\pi m_e)$. Here we have taken $f_c > 0$, but for Y_L and Y_T the negative charge of an electron is taken into account by the negative sign.

[19] As there is most likely a gradient of electron density N and collision frequency ν along the path of the SED radio wave, a complete treatment requires the solution of appropriate differential equations and such a full wave analysis is quite complicated. Nevertheless, for small gradients in N and ν with regard to the wavelength, the solution of Appleton's equation can give a good qualitative insight into the problem. Therefore we will compute this equation for typical parameters of N, f, f_c, ν, and θ in Saturn's ionosphere. Consequently, we will first examine the ranges of these five parameters for our data set of Cassini RPWS recorded radio waves of SEDs. It has already been mentioned that the frequency f of the SEDs in our data set goes only from 900 kHz to 1800 kHz (see Figure 3). In Figure 5 we have already illustrated the range of the angle θ, going from about 110° close to 180°, which is close to anti-parallel propagation. The vast majority of SED radio waves (586 out of 665 SED pixels) have $\theta > 135°$ and can be considered as close to longitudinal propagation against the magnetic field direction. It is well known that for longitudinal propagation an incident radio wave experiences two possible modes of propagation, which are circularly polarized with opposite senses of rotation. For arbitrary angles between radio wave direction and magnetic field there are two modes of elliptical polarization of opposite senses [*Kelso*, 1964]. This is consistent with our result of SED polarization measurements, which are elliptically polarized or nearly circularly polarized as many propagation angles are close to longitudinal propagation. However, for some reason which has to be figured out we can see only one sense of rotation.

[20] As a next quantity we determine the electron cyclotron frequency $f_c = |e|B/(2\pi m_e)$. Therefore we calculate the magnetic field strength B from a simple model of Saturn's dipole magnetic field with a magnetic moment of $M = 0.215$ R_S^3 Gauss [*Ness*, 1994]. We calculated the radial component of the magnetic field with the equation $B_r = 2M\cos(\phi)/r^3 = -0.237$ G and the latitudinal component using $B\phi = M\sin(\phi)/r^3 = 0.179$ G. In these equations ϕ is the colatitude of the (average) point where the radio wave passes the ionosphere measured from Saturn's rotational axis pointing northward, i. e. $\phi = 90 + 33.5 = 123.5°$. The distance r should be given in Saturn radii (R_S) and, including the oblateness of Saturn, an altitude of 2000 km at a planetocentric latitude 33.5° South is actually $r = 1.000$ R_S (equatorial Saturn radii) away from Saturn's center. As we have assumed a dipole in Saturn's center aligned along its rotation axis there is no azimuthal magnetic field component and no dependence of the magnetic field on the longitude. The total magnetic field strength at this position is $B = \sqrt{B_r^2 + B_\phi^2} = 0.297$ G, corresponding to an electron cyclotron frequency of $f_c \approx 830$ kHz. The variation of this value with altitude in Saturn's ionosphere can be neglected.

[21] Only the two remaining quantities of electron plasma density N and collision frequency ν are both functions of altitude and vary considerably along the path of the radio wave through the ionosphere. Altitude profiles for the electron density in Saturn's ionosphere have been measured with the Voyagers as well as Cassini by the method of radio occultation [*Lindal et al.*, 1985; *Nagy et al.*, 2006]. These profiles show a great variation with local time and latitude. Voyager 2 egress measurements were conducted in the early morning atmosphere at a planetographic latitude of 31.2° South [*Lindal et al.*, 1985]. This corresponds to a planetocentric latitude of 26.2° and is the measurement which comes closest to the local time and latitude of the SED storm from early 2006. Most electron density profiles show electron densities greater than 10^2 cm^{-3} from altitudes of 1000 km up to 3000 km or 4000 km, and the Voyager 2 egress profile at 31.2° South has a peak electron density of 10^4 cm^{-3} around 2000 km. That's why we have previously used the altitude of 2000 km as a mean ionospheric altitude to calculate the magnetic field as well as the various angles. On the other hand recent Cassini radio occultations at equatorial latitudes [*Nagy et al.*, 2006] have revealed different profiles for the dawn side with peaks only around 10^3 cm^{-3}. *Fischer et al.* [2007] determined the peak

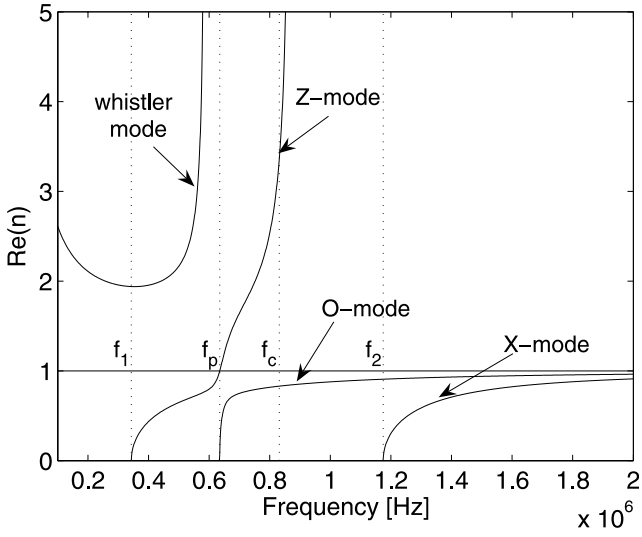

Figure 6. Real part of the refractive index n as a function of frequency for typical ionospheric conditions during SED measurements.

electron densities from the low frequency cutoff of the SED signals from storm E. They obtained values ranging from $3{\cdot}10^3$ to $3{\cdot}10^4$ cm^{-3} for local times from about 3 to 6 LT, which is the local time interval of most of SED signals from our data set (see Figure 5). We have chosen a value from the lower end of this range of $N = 5{\cdot}10^3$ cm^{-3}. This corresponds to an electron plasma frequency of $f_p = 635$ kHz.

[22] *Zarka* [1985] modeled the collision frequencies in Saturn's ionosphere and found that the collisions between electrons and ions are prevalent at typical ionospheric altitudes within an order of magnitude around $\nu_{e-i} = 10^3$ s^{-1}. This is a value assumed for the dayside of Saturn and it might be even smaller on the nightside. The shape of the dispersion relation is in fact only slightly dependent on the actual value of ν as long as $\nu \ll f$ which is most likely the case anyhow. The collision frequency ν influences the value of the imaginary part of the refractive index, but it will be shown later that the so-called absorption ratio is independent of ν as long as $\nu \ll f$.

[23] As an illustration we plot the refractive index n as a function of frequency f in Figure 6 by computing Appleton's equation using the following typical parameters, which we have discussed above: $N = 5{\cdot}10^3$ cm^{-3}, $f_c = 830$ kHz, $\nu = 10^3$ s^{-1}, and $\theta = 164°$ (median value of all θ in our data set). In Figure 6 we can identify the whistler mode, the Z-mode, and the "free space" ordinary mode (O-mode) and the extraordinary mode (X-mode), and the frequencies f_1 and f_2 are given by $f_{1,2} = \mp\frac{f_c}{2} + \sqrt{\frac{f_c^2}{4} + f_p^2}$. The whistler and Z-mode are trapped and below the frequency range of SED measurements and, hence, are of no interest to us here. Only the O-mode and the X-mode are accessible from free space and can be detected also from outside of Saturn's magnetosphere like the SEDs. The variation of the peak electron density N_{peak} (and not its variation along the raypath) influences the cutoff frequencies of O-mode and X-mode, which are f_p and f_2, respectively. With $N_{peak} = 10^3$ cm^{-3} we get $f_p \approx 280$ kHz and $f_2 \approx 920$ kHz, whereas for $N_{peak} = 10^4$ cm^{-3} we have $f_p \approx 900$ kHz and $f_2 \approx 1.4$ MHz, but the general shape of the refractive index for both "free space" modes is practically unchanged.

[24] Interestingly, between the plasma frequency $f_p \approx 635$ kHz and the cutoff frequency of the X-mode $f_2 \approx 1170$ kHz only the O-mode is present. We have to be cautious with the sense of rotation of X and O-mode: In the sense of plasma physics the rotation is defined with regard to the positive direction of the magnetic field, and the O-mode would be left-handed (LH) polarized in case the wave vector $\vec{k}$ has a positive component in magnetic field direction [see, e.g., *Gurnett and Bhattacharjee*, 2005]. However, as $\vec{k}$ is nearly antiparallel to $\vec{B}$, in our case the O-mode is right-handed (RH) and the X-mode is left-handed (LH) polarized in the IRE-definition. Figure 3 shows that the degree of circular polarization seems to be close to $\nu = -1$ up to 1200–1300 kHz, consistent with an elliptically polarized RH wave which is nearly purely circularly polarized with only a small degree of linear polarization. This is consistent with the RH polarization of the O-mode we inferred from the dispersion relation. Above f_2 both modes are present. However, plotting the absorption coefficient κ as a function of frequency in Figure 7 one can see that both modes have absorption coefficients which differ by about one order of magnitude above f_2. This will be investigated more closely in the next subsection. The absorption coefficient κ can be calculated from the imaginary part of the refractive index n with the equation $\kappa = -\frac{2\pi f}{c} Im(n)$ with c as the vacuum speed of light. Also, since there are two solutions for the refractive index n corresponding to the upper and lower sign of the dispersion relation, there are also two different κ. The upper sign (solid line) corresponds to the O-mode and whistler mode, whereas the lower sign (dashed line) corresponds to the X-mode and Z-mode. To be precise, the refractive index n is not absolutely zero for the X-mode between f_p and f_2, but it is so close to zero that it cannot be seen in Figure 6. Figure 7 shows that the attenuation of the X-mode is extremely high

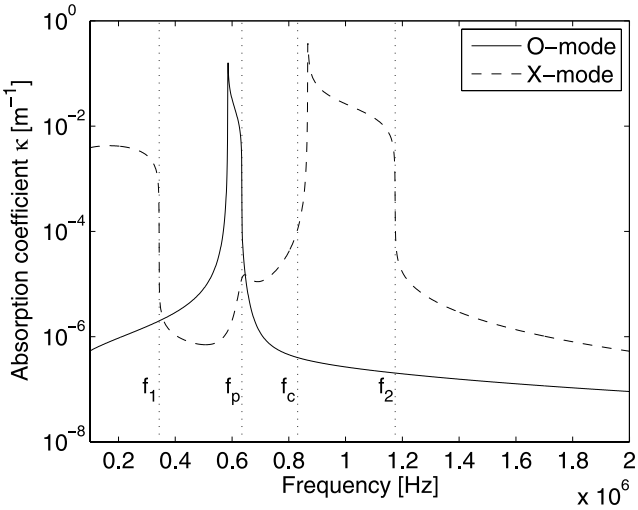

Figure 7. Absorption coefficient κ for O-mode and X-mode of the dispersion relation as a function of frequency for typical ionospheric conditions during SED measurements.

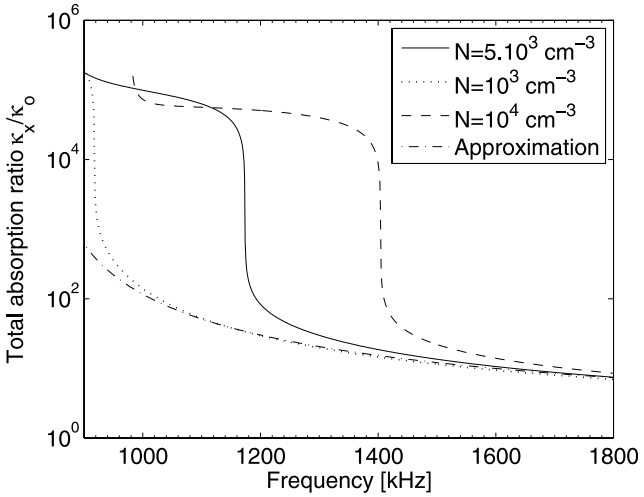

Figure 8. Total absorption ratio κ_x/κ_o between X- and O-mode as a function of frequency and the electron density N as parameter. The dash-dotted line is a quasilongitudinal approximation.

in this frequency interval, that our previous statement about the existence of only one mode between f_p and f_2 is correct for all practical purposes.

5.3. Differential Absorption Effect

[25] The previously noted difference in absorption coefficients between both modes can be called a differential absorption effect. Generally, the absorption of radio waves can be described by an exponential decay in electric field magnitude E from its initial value E_i by the following equation

$$E = E_i \exp\left(-\int \kappa ds\right) \tag{7}$$

with κ as the absorption coefficient which is integrated along the raypath. We can define the total absorption A by applying the logarithm to the equation above yielding

$$\begin{aligned} A &= 20\log\left(\frac{E}{E_i}\right) = 20\log\left[\exp\left(-\int \kappa ds\right)\right] \\ &= 20\log(e)\left(-\int \kappa ds\right) < 0. \end{aligned} \tag{8}$$

[26] As the wave intensity is proportional to the amplitude squared we have multiplied by 20, and as $\kappa > 0$, $E < E_i$, the absorption A should be a negative number given in dB. Equation (7) can be applied to the O-mode as well as to the X-mode and assuming that the initial field strength of O and X-mode are the same ($E_{i,o} = E_{i,x}$) one can make the following calculation

$$A_x - A_o = 20\log\left(\frac{E_x}{E_{x,i}}\right) - 20\log\left(\frac{E_o}{E_{o,i}}\right) = 20\log\left(\frac{E_x}{E_o}\right). \tag{9}$$

[27] In the following we derive another identity, where for simplicity we assume a unique absorption over the raypath and replace the integral $\int \kappa ds$ simply by $\kappa\Delta s$:

$$\frac{A_x}{A_o} = \frac{20\log(e)\left(-\int \kappa_x ds\right)}{20\log(e)\left(-\int \kappa_o ds\right)} \approx \frac{\kappa_x \Delta s}{\kappa_o \Delta s} = \frac{\kappa_x}{\kappa_o}. \tag{10}$$

[28] Hence the ratio of the total absorptions of X- and O-mode is given as the ratio of the absorption coefficients. We shall refer to this ratio simply as the total absorption ratio. With the last two equations it is easy to set up the following equation:

$$\frac{E_x}{E_o} = 10^{\frac{A_x - A_o}{20}} = 10^{\frac{A_o\left(\frac{\kappa_x}{\kappa_o} - 1\right)}{20}}. \tag{11}$$

[29] In Figure 8 we have plotted the total absorption ratio κ_x/κ_o as a function of frequency, and for the solid line with $N = 5 \cdot 10^3$ cm^{-3} we have used the previously calculated absorption coefficients from Figure 7 representing typical ionospheric conditions on Saturn's nightside during SED measurements. However, we have to be aware that we have a certain range of the ionospheric parameters of electron density N, collision frequency ν, and angle θ, which could also have an influence on the absorption ratio κ_x/κ_o. Via variation of parameters we found that the angle θ has practically no influence on the total absorption ratio and also the influence of the collision frequency is negligible as long as $\nu \ll f$. This can be seen easily using the formula for the absorption coefficient κ of the quasilongitudinal approximation as given by *Ratcliffe* [1959]:

$$\kappa = \frac{e^2 N \nu}{2\varepsilon_0 m_e c \mu \left[4\pi^2 (f \pm f_c)^2 + \nu^2\right]}, \tag{12}$$

where all symbols have been explained throughout the text except $\mu = Re(n)$ being the refractive index. The plus sign stands for the O-mode, whereas the minus sign is attributed to the X-mode, and in the latter case the attenuation has a maximum at the electron cyclotron frequency f_c. We can get the total absorption ratio κ_x/κ_o by a simple division:

$$\frac{\kappa_x}{\kappa_o} = \frac{\mu_o \left[4\pi^2 (f + f_c)^2 + \nu^2\right]}{\mu_x \left[4\pi^2 (f - f_c)^2 + \nu^2\right]}, \tag{13}$$

where μ_x and μ_o represent the refractive index of the X- and O-mode, respectively. As long as $\nu \ll f$, the total absorption ratio is practically independent from the actual value of the collision frequency. Only the absolute values of κ for each mode (Figure 7) are strongly influenced by the choice of ν, but not their ratio κ_x/κ_o. For the dash-dotted curve in Figure 8 we have set $\mu_o = \mu_x$, and one can see that this quasilongitudinal approximation gives good results for certain frequency ranges depending on the electron density N. Using Appleton's equation we calculated three different curves of the total absorption ratio using the electron densities N of 10^3, $5{\cdot}10^3$, and 10^4 cm^{-3}. These different electron densities result in different cutoff frequencies for the X-mode $f_2 = \frac{f_c}{2} + \sqrt{\frac{f_c^2}{4} + f_p^2}$ of 920, 1170, and 1400 kHz in

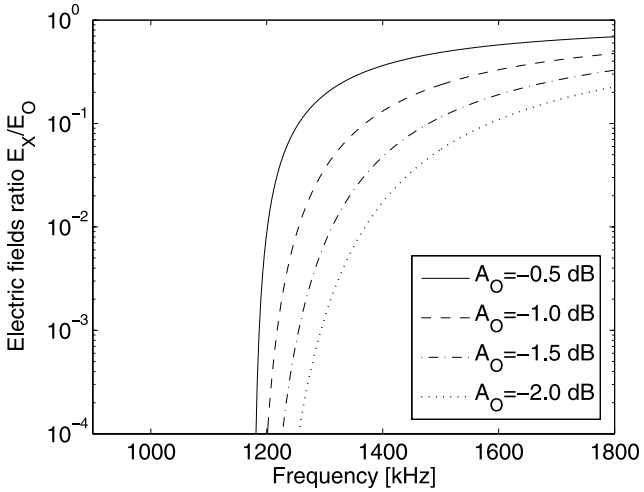

Figure 9. Wave electric field ratio E_x/E_o of X-mode to O-mode as a function of frequency with the total absorption of the O-mode A_o as parameter. A_o is varied from -0.5 dB to -2.0 dB and is drawn in different line styles.

ascending order. It can be seen that for frequencies $f > f_2$ the total absorption ratio is well approximated by the dash-dotted line, because as long as $\mu_x \approx \mu_o \approx 1$ the last equation shows no dependence of κ_x/κ_o from N, and the total absorption ratio is practically constant all along the raypath. Similarly, for electron densities $N < 10^3$ cm^{-3} the total absorption ratio is well approximated by the dash-dotted line, because the cutoff frequency of the X-mode f_2 comes close to $f_c \approx 830$ kHz and all SEDs of our data set have frequencies greater than f_c. The electron density N essentially influences only the value of the frequency f_2 below which the total absorption ratio jumps to a much higher value. In the case of $f < f_2$ and $N > 10^3$ cm^{-3} somewhere along the raypath the total absorption ratio has a lower limit given by the approximation of the dash-dotted line in Figure 8 and an upper limit given by the much higher values of about $\kappa_x/\kappa_o \approx 10^5$, which essentially means that the X-mode is practically completely absorbed.

[30] We can now model the ratio of wave electric fields of X and O-mode as a function of frequency. We take the second identity of equation (11) and insert the total absorption ratio κ_x/κ_o as a function of frequency with the electron density $N = 5 \cdot 10^3$ cm^{-3}. The total absorption of the ordinary wave mode A_o is taken as a parameter. Thereby we assume that A_o does not vary much with frequency, which is a reasonable approximation as κ_o is approximately constant above f_c which can be seen in Figure 7. The E_x/E_o ratio should be much smaller than 1 close to f_2, as the X-mode experiences much more attenuation than the O-mode, resulting in a dominance of the O-mode which in our case has a RH rotation sense. The amplitude ratio E_x/E_o is plotted in Figure 9 as a function of frequency with the total absorption of the O-mode A_o as a parameter varying from -0.5 to -2.0 dB, and it will become clear later why we chose that range.

5.4. Superposition of LH and RH Mode Wave

[31] The RPWS antenna system measures the Stokes parameters of the superposition of the LH and RH mode wave. The two modes have to be treated as independent waves (we will justify this point toward the end of this section) propagating in the same direction and the resultant wave is the sum of the Stokes parameters of the individual waves. In the following equation we sum up two elliptically polarized waves with different rotation senses. In the appendix of this paper it is shown that if the LH mode is given by the normalized Stokes parameters (q, u, v) (with $v > 0$) the corresponding RH mode is given by ($-q$, u, $-v$). However, due to the differential absorption effect in our case both modes have different intensities S_L and S_R (intensity of LH and RH mode, respectively). Hence we make the following summation using four-component vectors:

$$S_L \begin{pmatrix} 1 \\ q \\ u \\ v \end{pmatrix} + S_R \begin{pmatrix} 1 \\ -q \\ u \\ -v \end{pmatrix} = \begin{pmatrix} S_L + S_R \\ q(S_L - S_R) \\ u(S_L + S_R) \\ v(S_L - S_R) \end{pmatrix} \tag{14}$$

[32] Using equations (4) it is straightforward to derive the linear polarization degree d_l as well as the circular one d_c of the resultant wave:

$$d_l = \frac{\sqrt{q^2(S_L - S_R)^2 + u^2(S_L + S_R)^2}}{S_L + S_R} = \sqrt{q^2\left(\frac{S_L - S_R}{S_L + S_R}\right)^2 + u^2} \tag{15}$$

$$d_c = v\frac{S_L - S_R}{S_L + S_R} = v\frac{\frac{S_L}{S_R} - 1}{\frac{S_L}{S_R} + 1} = v\frac{\left(\frac{E_L}{E_R}\right)^2 - 1}{\left(\frac{E_L}{E_R}\right)^2 + 1}. \tag{16}$$

with E_R and E_L as the RH and LH electric field amplitude, whose square is proportional to the wave intensity. These equations can now be used to model the circular and linear polarization degrees as a function of frequency, as we have derived the amplitude ratio $E_L/E_R = E_x/E_o$ as a function of frequency in the previous subsection. Therefore we first look at our lowest measurement frequencies, where we assume that only one mode is present. From Figure 3 we can see that the circular polarization is $d_c \approx -0.9$ below 1000 kHz. Similarly, we find from Figure 4 that the linear polarization is about $d_l = 0.3$ at the lowest measurement frequencies. This yields a total polarization of about 95% for these SEDs which we believe to be from the O-mode only. Theoretically, one single magneto-ionic mode is a completely polarized wave (100%), so the result of about 95% confirms the likely hypothesis that the SEDs between f_p and f_2 belong to one single mode. Figure 10 now shows our model for the circular polarization as a function of frequency using equation (16) by setting $v = 0.9$. Similarly, we can model the maximum change of linear polarization with frequency by putting all of the measured linear polarization into the parameter q, i.e., $q = 0.3$. (If all the linear polarization would be in the parameter u, there would be no variation of linear polarization with frequency according to equation (15).) This is displayed in Figure 11, and one can see that even for the lowest total absorption of the O-mode (LH) of $A_o = -0.5$ dB there is only a moderate

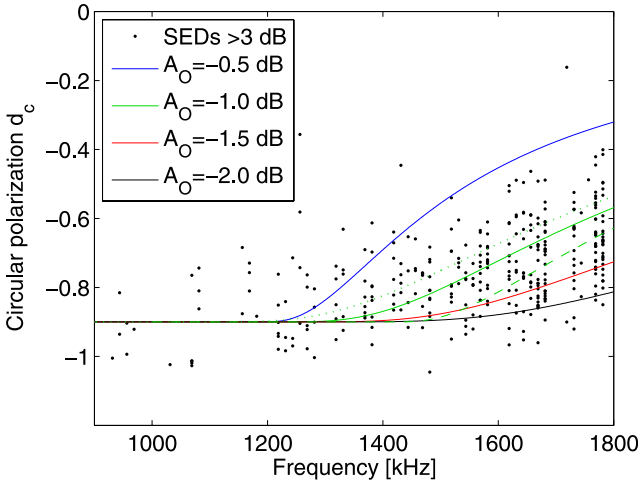

Figure 10. SED measurements of circular polarization d_c (black dots) and model curves as a function of frequency. For clarity we only took mean SEDs intensities (from dipole and monopole) greater than 3 dB above background. The model curves have the total absorption of the ordinary mode A_o varying from −0.5 dB to −2.0 dB as parameter. The solid model curves of d_c are plotted for an electron density of $N = 5{\cdot}10^3$ cm^{-3}. Only for $A_o = -1.0$ dB we have plotted the curves also for $N = 10^3$ cm^{-3} (dotted green line) and $N = 10^4$ cm^{-3} (dashed green line).

change of linear polarization as a function of frequency, which is still within the scatter of the measurement points. For clarity we have displayed only those SED measurement as points in Figures 10 and 11 that had mean intensities greater than 3 dB above background (mean intensity from both antennas E_x and E_w). The change of circular polarization as a function of frequency is clearly more evident, although there is also significant scatter. This scatter is only partly due to measurement errors as the scatter seems to get systematically larger with increasing frequency. Hence it might be mainly due to different amounts of total absorption A_o, and in fact the scatter can be attributed to a fairly realistic variation of A_o from −0.5 dB to −2.0 dB. This slight variation of total absorption of the O-mode can be due to different ionospheric conditions at different Saturn rotations, different local times of the SED storm on the nightside, and of course also different angles of incidence of the $\vec{k}$−vector with regard to the ionospheric normal (see Figure 5) leading to longer and shorter raypaths within the absorbing medium. Furthermore, as the SEDs come from different local times at the night side of Saturn, different electron densities N are involved. All solid lines in Figures 10 and 11 are plotted for an electron density of $N = 5{\cdot}10^3$ cm^{-3}. Only for the total absorption of $A_o = -1.0$ dB we have also plotted the modeled circular and linear polarization for electron densities of 10^3 cm^{-3} (dotted green line), and 10^4 cm^{-3} (dashed green line).

[33] The two magnetoionic modes can be treated as independent (incoherent) or dependent (coherent) waves, and there is a considerable difference between these two treatments. By adding the Stokes parameters two oppositely circularly polarized waves add up to an unpolarized wave, whereas adding the wave amplitudes for coherent modes would lead to a linear polarized composite signal (e.g., Faraday effect). Our polarization measurements have shown that rather the former is the case and this can be understood in the following way. The largely different refractive indices between O-mode and X-mode below 2 MHz imply different phase and group velocities of the two modes leading to different arrival times at the Cassini antennas. Calculating the group velocities by using the refractive indices as given in Figure 6 and assuming a thickness of the ionosphere of 1500 km leads to an O-mode signal arriving several milliseconds prior to the X-mode. For 1.2 MHz this time difference is about 100 ms, whereas for 1.8 MHz it goes down to about 1 ms (due to the largely different refractive indices). Although the total duration of an SED can sometimes be several hundred milliseconds, it is likely that an SED is made up of several short sub-pulses [*Farrell et al.*, 2007] similar to a terrestrial lightning flash. These subpulses are most likely shorter than the arrival time difference between the two modes, hence there is no adding up of wave amplitudes.

[34] We note that the measured degree of linear polarization around $d_l \approx 0.3$ is probably too high due to an instrumental effect of the RPWS-HFR, as already noted by *Cecconi et al.* [2006]. They found a 0.1 linear polarization degree bias in the upper frequency range of the SKR (Saturn Kilometric Radiation). We plotted spectra of apparent polarization and found that even the unpolarized background has a linear polarization degree of 0.5 in the HF1 receiver above the SKR frequencies where the SEDs are located. In fact, besides the dispersion relation we also computed the so-called polarization equation [*Ratcliffe*, 1959; *Kelso*, 1964; *Budden*, 1985] and found that the linear polarization degree of the SEDs should theoretically be smaller than 0.05 for frequencies greater 1 MHz and angles $\theta > 160°$ (regarding θ see Figure 5). Nevertheless, also the polarization equation yields an approximately constant degree of linear polarization for both modes above 1 MHz far from the plasma frequency.

[35] In summary, the applied magneto-ionic theory can clearly explain the polarization properties of SEDs. The

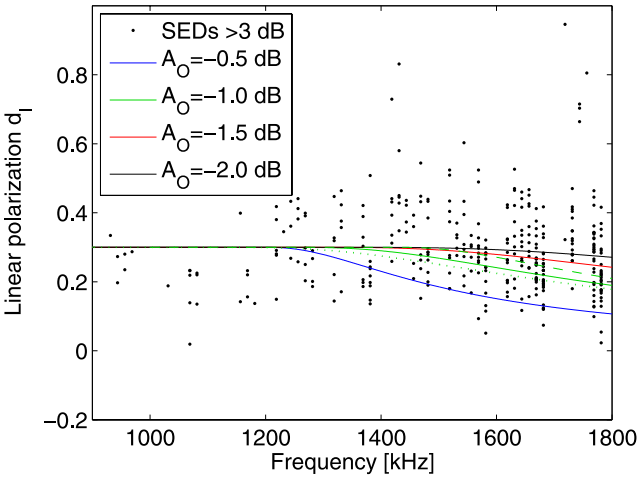

Figure 11. Similar to Figure 10, only for SED measurements of linear polarization d_l and corresponding model curves as a function of frequency.

exclusively RH sense of SED polarization in the HF1 band is due to the presence of only one magneto-ionic mode (the O-mode) from the plasma frequency up to about 1200 kHz, the cutoff frequency of the X-mode. The continuing dominance of the O-mode (RH in our case) up to 1800 kHz is caused by a differential absorption effect. We are also able to understand and derive the approximately constant degree of linear polarization as well as the decrease in magnitude of circular polarization as a function of increasing frequency. The latter effect also gives us some clues about the absorption of ordinary mode radio waves in Saturn's nightside ionosphere, which should range from about -0.5 to -2.0 dB.

6. Discussion

[36] The results of the polarization measurements add another strong argument to the already long list of arguments presented by *Fischer et al.* [2007] that SEDs are nothing other than the radio signature of Saturnian lightning. Although we have assumed for the polarization measurement that Saturn has to be the source of the SEDs, the results plus their interpretation with magneto-ionic theory implies a source that has to be below Saturn's ionosphere, and most likely in Saturn's atmosphere. We have also calculated the apparent polarization (which inherently assumes a source direction perpendicular to the antenna plane) for our data set of SEDs and except for the sign flip in circular polarization the results are quite similar to the ones presented in section 4. Hence our measured SED bursts are highly polarized signals implying the involvement of a polarizing medium like Saturn's ionosphere. The occurrence of SEDs with a frequency below 2 MHz only when the ISS imaged cloud system is on the nightside of Saturn (see Figure 5) is in perfect agreement with our knowledge of ionospheric cutoff frequencies [*Kaiser et al.*, 1984; *Zarka*, 1985].

[37] It is also interesting to look at the following question: Are radio emissions from terrestrial lightning polarized? Polarization measurements of radio emissions from terrestrial lightning flashes in the frequency range of a few MHz have seldom been conducted or reported. Such measurements are difficult to perform on the ground due to the influence of the conducting Earth and surrounding structures, the latter having a similar length scale as decametric radio waves. Hence observations with satellites that are equipped with at least two antennas and additional cameras to locate the source are a good way to perform such measurements, although the influence of the ionosphere also has to be considered. *Shao and Jacobson* [2002] reported polarization measurements of lightning-produced VHF emissions with the FORTE satellite. For discharge processes like first return strokes, dart leaders, and K streamers no recognizable polarization was observed. However, the recently discovered TIPPs (Transionospheric Pulse Pairs) were found to be highly polarized. TIPPs are believed to be caused by narrow bipolar pulses that last a few microseconds and are related to intracloud discharges [*Smith et al.*, 1999]. Surprisingly, they have a relatively flat spectrum in HF and VHF [*Massey and Holden*, 1995; *Jacobson et al.*, 1999], which is also a characteristic feature of the SEDs [*Zarka and Pedersen*, 1983; *Farrell et al.*, 2007]. Each pulse of a TIPP showed two separate highly polarized regions in the dynamic spectrum below 40 MHz. They were elliptically polarized with different senses of polarization, and *Shao and Jacobson* [2002] identified them as the ordinary and extraordinary magneto-ionic mode. Because of the higher frequencies, no differential absorption effect was observed for the TIPPs and both modes had approximately the same intensity. However, as a result of the dispersion of the signal in the terrestrial ionosphere both modes arrived at the spacecraft at different times separated by only a few microseconds, and the very high time resolution of the FORTE radio receiver allowed a distinction between them up to 40 MHz. In case of the SEDs the time resolution of 40 ms and the sweeping nature of the RPWS/HFR does not allow a temporal separation of the two magneto-ionic modes and so RPWS can only measure the composite signal. Nevertheless, in this paper we have inferred the existence of the two modes from theoretical considerations. *Shao and Jacobson* [2002] deduced that the two magneto-ionic modes come from an originally linearly polarized signal at the source due to a straight discharge path, which is also supported by the Faraday rotation they observed. In case of the SEDs the small bandwidth of the sweeping receiver does not allow an observation of Faraday rotation, but just like TIPPs also SEDs might be linearly polarized at the source. It is worth noting that TIPPs are an interesting analogy to SEDs as they share the following four characteristic properties. Both of them are (1) related to intracloud lightning, (2) are strong radiators in HF (high frequency) and VHF (very HF), (3) have a flat spectrum in HF and VHF, and (4) both have a high degree of circular polarization introduced by the dispersion in the magneto-plasma of the respective ionosphere.

[38] Our explanation of the polarization of SEDs in the frame of magneto-ionic theory might get additional support from possible future Saturn lightning observations with Cassini. In case the lightning source can be identified in Saturn's Northern hemisphere and Cassini is in an appropriate position, the wave vector $\vec{k}$ would have a positive component in magnetic field direction. Hence the O-mode SEDs should exhibit a LH polarization (below 2 MHz) with regard to $\vec{k}$, which would be the opposite sense to the RH polarization we have detected now with the source at 35° South. In this sense it is interesting to reconsider the Voyager 1 SED measurements by *Evans et al.* [1981]. The most likely source of the Voyager SEDs was an equatorial storm [*Kaiser et al.*, 1983; *Zarka and Pedersen*, 1983], and the polarization measurements of *Evans et al.* [1981] were done for the first SED post-encounter episode of Voyager 1. At this time (a few hours around 12:00 SCET, DOY 318, 1980) the spacecraft was at a latitude a few degrees around 15° North. Hence the angle between the wave vector $\vec{k}$ and the magnetic field $\vec{B}$ should be greater than 90° by about 15° at Saturn's equatorial ionosphere. Consequently, the PRA should have observed SEDs of RH polarization, and according to Figure 5 of *Evans et al.* [1981] it actually did for frequencies in the PRA low-band receiver below 1.3 MHz. We can be quite sure that the PRA low-band frequencies are still in the quasistatic frequency range as the PRA antennas have the same length of 10 m [*Warwick et al.*, 1977] like the RPWS antennas. For higher frequencies the degree of polarization of the Voyager SEDs

turned gradually from RH to clearly LH at 15 MHz, but at such a high frequency the measurement result is most likely biased by instrumental effects. It might be interesting to see how the polarization evolves at higher frequencies for RPWS SED measurements. From theory we would expect an increasing depolarization of the composite signal as the differential absorption effect gets less pronounced with increasing frequency. Naturally, we have to face the same problem of getting gradually out of the quasistatic regime into a frequency range where our antenna calibration is not valid anymore. However, we might overcome this problem by a computational wire-grid modeling of the RPWS antenna system and the spacecraft [*Fischer et al.*, 2001], which can also determine the effective length vectors at higher frequencies.

7. Conclusions

[39] Cassini/RPWS has performed polarization measurements of SEDs in the HF1 band of its High Frequency Receiver below a frequency of 2 MHz during an SED storm early in 2006. In this frequency range the RPWS antenna system is fully calibrated, and we have included the antenna-source geometry in the measurement, assuming Saturn to be the source. Our data set consisted of SEDs that were presumably radiated when a prominent convective cloud system located at a planetocentric latitude of 35° South was located on the nightside of Saturn. The polarization measurements have shown that SEDs are highly polarized (~80%) below 2 MHz with a particular high degree of circular polarization (~70% on average). They showed exclusively one sense of rotation, which was right-handed (RH) in the radioastronomical sense. Additionally we have found a decrease of the magnitude of circular polarization $|d_c|$ with increasing frequency f from 900–1800 kHz. The linear polarization clearly has a lower level and seems to be rather constant with frequency.

[40] The polarization measurements can be well explained in the frame of magneto-ionic theory. First, there are different cutoff frequencies for the LH and RH mode in the magnetoplasma of Saturn's ionosphere. Secondly, a differential absorption effect leads to different attenuation of the LH and RH mode. The resulting different wave intensities can directly explain the change of circular polarization with frequency. We note an interesting analogy between SEDs and the highly polarized TIPP events, the latter caused by terrestrial intracloud strokes.

Appendix A: Wave Polarization of Magneto-ionic Modes

[41] In this appendix we will describe the wave polarization of the two magneto-ionic modes in terms of the Stokes parameters. In magneto-ionic theory the polarization is usually described by a single complex number p, which is defined as the ratio of the components of the wave magnetic field H in the x′ and y′ direction, respectively [*Budden*, 1985]:

$$p = Re(p) + jIm(p) = -\frac{H_{x'}}{H_{y'}} = \frac{E_{y'}}{E_{x'}}. \tag{A1}$$

[42] The complex quantity p has a real part and an imaginary part and can be also expressed as ratio of the components of the wave electric field E. The coordinate axis y′ is normally chosen transverse to the direction of the ambient magnetic field, and x′ is perpendicular to y′ as well as perpendicular to the direction z′ of wave propagation. It can be shown [*Ratcliffe*, 1959; *Kelso*, 1964; *Budden*, 1985] that the polarization of the ordinary and extraordinary mode, p_o and p_x (or LH and RH mode, p_L and p_R) are related by the simple equation

$$p_o p_x = p_L p_R = 1. \tag{A2}$$

[43] The description of the polarization state with the two numbers ($Re(p)$, $Im(p)$) implies completely polarized waves. On the contrary, the description of polarization with the four Stokes parameters (I, Q, U, V) can be also used for partly polarized waves and we do have the additional information about the wave intensity. The normalized Stokes parameters (q, u, v) are given by *Mott* [1986] as a function of the polarization p:

$$q = \frac{1-|p|^2}{1+|p|^2}, u = \frac{2Re(p)}{|p|^2+1}, v = \frac{2Im(p)}{|p|^2+1} \tag{A3}$$

[44] Assuming that we do know the state of polarization of one mode (e.g., the ordinary one) given by ($Re(p_o)$, $Im(p_o)$) or (q_o, u_o, v_o) it is possible to calculate the state of polarization ($Re(p_x)$, $Im(p_x)$) or (q_x, u_x, v_x) of the extraordinary mode. Setting $p_o = Re(p_o) + j\, Im(p_o)$ and $p_x = Re(p_x) + j\, Im(p_x)$ one can easily solve the equation $p_o\, p_x = 1$ for $Re(p_x)$ and $Im(p_x)$ yielding

$$Re(p_x) = \frac{Re(p_o)}{|p_o|^2} \text{ and } Im(p_x) = -\frac{Im(p_o)}{|p_o|^2} \tag{A4}$$

[45] In terms of the Stokes parameters we can now make the following calculation using also the identity $|p_o p_x| = |p_o||p_x| = 1$:

$$\begin{aligned} q_o &= \frac{1-|p_o|^2}{1+|p_o|^2} = \frac{1-\frac{1}{|p_x|^2}}{1+\frac{1}{|p_x|^2}} \\ &= \frac{|p_x|^2-1}{|p_x|^2+1} = -\frac{1-|p_x|^2}{1+|p_x|^2} = -q_x \end{aligned} \tag{A5}$$

$$\begin{aligned} u_o &= \frac{2Re(p_o)}{|p_o|^2+1} = \frac{2|p_o|^2 Re(p_x)}{|p_o|^2+1} \\ &= \frac{2Re(p_x)}{1+\frac{1}{|p_o|^2}} = \frac{2Re(p_x)}{|p_x|^2+1} = u_x \end{aligned} \tag{A6}$$

$$\begin{aligned} v_o &= \frac{2Im(p_o)}{|p_o|^2+1} = \frac{-2|p_o|^2 Im(p_x)}{|p_o|^2+1} \\ &= -\frac{2Im(p_x)}{1+\frac{1}{|p_o|^2}} = -\frac{2Im(p_x)}{|p_x|^2+1} = -v_x \end{aligned} \tag{A7}$$

[46] The polarization ellipses of the two modes are often graphically displayed in the plane of the wavefront [see, e.g., *Kelso*, 1964 or *Ratcliffe*, 1959], and one can be obtained from the other by reflecting it along a line which is tilted by 45° from the coordinate axis x′ toward y′. We have seen that the two modes are completely polarized waves with opposite senses of rotation, and in terms of the Stokes parameters one mode described by (q, u, v) has a corresponding second mode given by ($-q$, u, $-v$). This result is used to set up equation (14) in section 5.

[47] **Acknowledgments.** Amitava Bhattacharjee thanks Steven Desch and Abram Jacobson for their assistance in evaluating this paper.

References

Budden, K. G. (1985), *The propagation of radio waves*, Cambridge Univ. Press, Cambridge, Great Britain.

Cecconi, B., and P. Zarka (2005), Direction finding and antenna calibration through analytical inversion of radio measurements performed using a system of 2 or 3 electric dipole wire antennas, *Radio Sci.*, *40*(3), RS3003, doi:10.1029/2004RS003070.

Cecconi, B., P. Zarka, and W. S. Kurth (2006), SKR polarization and source localization with the Cassini/RPWS/HFR instrument: First results, in *Planetary Radio Emissions VI*, edited by H. O. Rucker, W. S. Kurth, and G. Mann, Austrian Academy of Sciences Press, Vienna, 37–49.

Dyudina, U. A., A. P. Ingersoll, P. E. Shawn, C. C. Porco, G. Fischer, W. S. Kurth, M. D. Desch, A. Del Genio, J. Barbara, and J. Ferrier (2007), Lightning storms on Saturn observed by Cassini ISS and RPWS during 2004–2006, *Icarus*, *190*, 545–555.

Evans, D. R., J. W. Warwick, J. B. Pearce, T. D. Carr, and J. J. Schauble (1981), Impulsive radio discharges near Saturn, *Nature*, *292*, 716–718.

Farrell, W. M., M. L. Kaiser, G. Fischer, P. Zarka, W. S. Kurth, and D. A. Gurnett (2007), Are Saturn Electrostatic Discharges really superbolts? A temporal dilemma, *Geophys. Res. Lett.*, *34*, L06202, doi:10.1029/2006GL028841.

Fischer, G., W. Macher, H. O. Rucker, H. P. Ladreiter, D. F. Vogl, and the Cassini RPWS Team (2001), Wire–Grid modeling of Cassini spacecraft for the determination of effective antenna length vectors of the RPWS antennas, in *Planetary Radio Emissions V*, edited by H. O. Rucker, M. L. Kaiser, and Y. Leblanc, Austrian Academy of Sciences Press, Vienna, 347–356.

Fischer, G., W. Macher, H. O. Rucker, and the Cassini/RPWS team (2003), Reception properties of the Cassini/RPWS antennas from 1 to 16 MHz. Poster presentation at the EGS-AGU Joint Assembly, Nice, France.

Fischer, G., M. D. Desch, P. Zarka, M. L. Kaiser, D. Gurnett, A. Kurth, W. S. Macher, W. Rucker, H. O. Lecacheux, A. W. M. Farrell, and B. Cecconi (2006), Saturn lightning recorded by Cassini/RPWS in 2004, *Icarus*, *183*, 135–152.

Fischer, G., W. S. Kurth, U. A. Dyudina, M. L. Kaiser, P. Zarka, A. Lecacheux, A. P. Ingersoll, and D. A. Gurnett (2007), Analysis of a giant lightning storm on Saturn, *Icarus*, *190*, 528–544.

Gurnett, D. A., and A. Bhattacharjee (2005), *Introduction to Plasma Physics*, Cambridge Univ. Press, Cambridge, Great Britain.

Gurnett, D. A., et al. (2004), The Cassini radio and plasma wave science investigation, *Space Sci. Rev.*, *114*, 395–463.

Jacobson, A. R., S. O. Knox, R. Franz, and C. D. Enemark (1999), FORTE observations of lightning radio-frequency signatures: capabilities and basic results, *Radio Sci.*, *34*, 337–354.

Kaiser, M. L., J. E. P. Connerney, and M. D. Desch (1983), Atmospheric storm explanation of Saturnian electrostatic discharges, *Nature*, *303*, 50–53.

Kaiser, M. L., M. D. Desch, and J. E. P. Connerney (1984), Saturn's ionosphere: Inferred electron densities, *J. Geophys. Res.*, *89*(A4), 2371–2376.

Kelso, J. M. (1964), *Radio ray propagation in the ionosphere*, McGraw–Hill book company, New York, USA.

Kraus, J. D. (1986), *Radio Astronomy*, 2nd edition, Cygnus–Quasar Books, Powell, Ohio.

Lindal, G. F., D. N. Sweetnam, and V. R. Eshleman (1985), The atmosphere of Saturn: An analysis of the Voyager radio occultation measurements, *Astron. J.*, *90*, 1136–1146.

Massey, R. S., and D. N. Holden (1995), Phenomenology of transionospheric pulse pairs, *Radio Sci.*, *30*(5), 1645–1659.

Mott, H. (1986), *Polarization in antennas and radar*, John Wiley and Sons, New York.

Nagy, A. F., et al. (2006), First results from the ionospheric radio occultations of Saturn by the Cassini spacecraft, *J. Geophys. Res.*, *111*(A6), A06310, doi:10.1029/2005JA011519.

Ness, N. F. (1994), Intrinsic magnetic fields of the planets: Mercury to Neptune, *Phil. Trans. R. Soc. Lond. A*, *349*, 249–260.

Ortega-Molina, A., and G. Daigne (1984), Polarization response of two crossed monopoles on a spacecraft, *Astron. Astrophys.*, *130*, 301–310.

Ratcliffe, J. A. (1959), *The magneto–ionic theory and its applications to the ionosphere*, Cambridge Univ. Press, Cambridge, Great Britain.

Rucker, H. O., W. Macher, R. Manning, and H. P. Ladreiter (1996), Cassini model rheometry, *Radio Sci.*, *31*(6), 1299–1311.

Shao, X. M., and A. R. Jacobson (2002), Polarization observations of lightning–produced VHF emissions by the FORTE satellite, *J. Geophys. Res.*, *107*(D20), 4430, doi:10.1029/2001JD001018.

Smith, D. A., X. M. Shao, D. N. Holden, C. T. Rhodes, M. Brook, P. R. Krehbiel, M. Stanley, W. Rison, and R. J. Thomas (1999), A distinct class of isolated intracloud lightning discharges and their associated radio emissions, *J. Geophys. Res.*, *104*(D4), 4189–4212.

Vogl, D. F., et al. (2004), In-flight calibration of the Cassini-Radio and Plasma Wave Science (RPWS) antenna system for direction-finding and polarization measurements, *J. Geophys. Res.*, *109*, A09S17, doi:10.1029/2003JA010261.

Warwick, J. W., J. B. Pearce, R. G. Peltzer, and A. C. Riddle (1977), Planetary radio astronomy experiment for Voyager missions, *Space Sci. Rev.*, *21*, 309–327.

Warwick, J. W., et al. (1981), Planetary radio astronomy observations from Voyager 1 near Saturn, *Science*, *212*, 239–243.

Zarka, P. (1985), Directivity of Saturn Electrostatic Discharges and ionospheric implications, *Icarus*, *61*, 508–520.

Zarka, P., and B. M. Pedersen (1983), Statistical study of Saturn Electrostatic Discharges, *J. Geophys. Res.*, *88*(A11), 9007–9018.

Zarka, P., B. Cecconi, and W. S. Kurth (2004), Jupiter's low-frequency radio spectrum from Cassini/Radio and Plasma Wave (RPWS) absolute flux density measurements, *J. Geophys. Res.*, *109*, A09S15, doi:10.1029/2003JA010260.

G. Fischer, D. A. Gurnett, and W. S. Kurth, Department of Physics and Astronomy, University of Iowa, 203 Van Allen Hall, Iowa City, IA 52242, USA. (georg-fischer@uiowa.edu)

A. Lecacheux, Observatoire de Paris-Meudon, 5 Place Jules Janssen, 92195, Meudon Cedex, France.

W. Macher, Space Research Institute, Austrian Academy of Sciences, Schmiedlstr. 6, A-8042 Graz, Austria.